Volume 19, Number 1, 2026. pp. 75-83

Jordan Journal of Physics

ARTICLE

Laser and Aluminum-Induced Crystallization of Amorphous Silicon Thin Films: Influence of Power Density and Layers Stacking Configuration

Adnan Shariah and **Ahmad Almasri**

Physics Department, Jordan University of Science and Technology, P.O. Box 3030, 22110, Irbid, Jordan.

DOI: **https://doi.org/10.47011/19.1.8**

Received on: 02/06/2025; *Accepted on: 19/02/2026*

Abstract: This study examines the crystallization of sputtered amorphous silicon (a-Si) thin films in contact with aluminum thin films on Corning glass substrates under continuous-wave (CW) laser irradiation. The study reveals key factors that affect the transition from amorphous to polysilicon by varying laser power densities and exposure durations. The crystallinity was assessed by Raman spectroscopy, while the surface morphology and structural alterations were examined using scanning electron microscopy (SEM). The results demonstrate that crystallization occurs beyond a certain threshold power density, with the creation of polysilicon being enhanced by increased laser intensity and longer exposure time. The results also show that the stacking order of silicon and aluminum layers directly affects crystallization behavior. This aspect has not been previously explored. These results improve understanding of laser-induced aluminum-mediated crystallization, which has implications for optoelectronic applications and thin-film technologies.

Keywords: Crystallization, Amorphous silicon, Continuous-wave laser, Aluminum-induced process, Laser power density, Optoelectronics, Thin films.

PACS-6 Code (61.43.Dq Amorphous semiconductors, metals, and alloys) (81.40.Ef Heat treatment, annealing) (81.40.Tv Optical treatment of materials) (81.10.-h Methods of crystal growth; physics and chemistry of crystal growth).

Introduction

Silicon is one of the most common elements on Earth and has been the basis of the semiconductor industry for many years. The material's versatility and unique characteristics make it an ideal substance for a wide range of applications, including microelectronics and photovoltaics [1, 2].

Amorphous silicon (a-Si) is considerably different from its crystalline counterpart in terms of its optical and electrical properties, as it demonstrates a distinct lack of long-range atomic ordering. a-Si's efficacy in numerous applications is compromised in comparison to crystalline silicon (c-Si), despite the fact that it offers certain advantages, such as the ability to be deposited on flexible substrates and reduced production costs. To reduce the performance gap between amorphous and crystalline silicon, researchers have explored methods for crystallizing amorphous silicon thin films. The primary objective is to effectively combine the benefits of both amorphous and crystalline structures [3, 4].

Laser annealing techniques are a promising approach to the crystallization of a-Si thin coatings. In particular, continuous-wave (CW) laser crystallization has garnered significant attention as a preferred method due to its ability to provide localized heating, precise control over the crystallization process, and the potential for scalable, large-area processing [5, 6]. CW laser crystallization offers several advantages over

Corresponding Author: Adnan Shariah **Email**: shariah@just.edu.jo

alternative techniques, such as furnace annealing and pulsed laser annealing, including a reduced thermal budget, improved control over grain size, and the ability for selective area crystallization, thus providing a more precise and effective method for crystallizing a-Si thin films [7]. This approach is distinguished by its energy efficiency, an essential aspect of modern production processes. CW systems provide a continuous flow of laser energy, therefore reducing energy waste and enhancing heat distribution across the target material [8]. The careful regulation of process parameters, such as laser power density, exposure duration, and beam profile, facilitates the optimization of the crystallization process [9]. These customizable characteristics allow researchers to tailor grain size and orientation, which is crucial for improving the performance of electrical devices like solar cells and displays [10]. The integration of energy efficiency and parameter regulation renders CW an essential technique in the fabrication of sophisticated thin film technologies, advancing the frontiers of semiconductor and optoelectronic applications [11].

A recent study by Shariah [12] investigated the crystallization of hydrogenated amorphous silicon (a-Si:H) films deposited on glass substrates via plasma-enhanced chemical vapor deposition (PECVD), using a combined approach of continuous wave (CW) laser irradiation and aluminum-induced thermal annealing. The experimental protocol involved exposing hydrogenated a-Si films to CW laser irradiation at different power densities and variable durations, followed by thermal annealing at 250 °C for 15 min. Scanning electron microscopy (SEM) and X-ray diffraction (XRD) analyses revealed that the laser power density, radiation duration, and thermal annealing conditions significantly affected the formation, shape, and amount of polycrystalline silicon (Poly-Si) grains within the film. The results showed that large Poly-Si grains could be generated under certain conditions, with the aluminum-induced thermal annealing step playing an essential role in promoting crystallization, even at relatively low temperatures. In other studies, Shariah and his colleagues investigated the aluminum-induced thermal crystallization of a-Si thin films, resulting in the production of high-quality polysilicon films at low processing temperatures [13, 14].

Park et al. [15] examined the microstructural evolution of island-patterned amorphous silicon (a-Si) thin films subjected to CW laser crystallization. The study focused on the influence of key process parameters, specifically the a-Si film thickness and the width of Si islands, on the resulting crystalline structure. Through rigorous analysis, the researchers observed a significant correlation between these parameters and the average grain boundary spacing, which serves as a proxy for grain size. Their findings revealed that both the thickness of the a-Si film and the width of the Si islands exert a strong influence on the final grain dimensions.

The objective of this research is to investigate the influence of continuous wave laser radiation with varying power densities on the crystallization process of sputtered a-Si thin layers, without the necessity of thermal annealing. The laser-induced crystallization of a-Si in contact with aluminum thin films is characterized in this study through the utilization of Raman spectroscopy and scanning electron microscopy (SEM). A quantitative evaluation of the crystalline percentage is achieved by the measurement of silicon phonon modes using Raman spectroscopy. On the other hand, SEM provides insights into surface morphology and grain structure. It is possible to optimize processing conditions by correlating crystallinity with grain morphology as a function of laser power density, irradiation time, and layer sequence. This allows for the improvement of grain quality and the reduction of defects. The result is an improvement in the electrical and optical properties of the produced polysilicon films, which can be used for thin-film fabrication and optoelectronic applications. This study aims to provide comprehensive insights into the crystallization process and its impact on the material properties.

Experimental Technique

The a-Si films were prepared using the same experimental procedure as in our previously published work [13, 14]. Corning glass 7059 was employed as the substrate for the deposition of sputtered a-Si films. The glass substrate was thoroughly cleaned in an ultrasonic chemical bath prior to the deposition procedure. A DC magnetron sputtering technique was used to

deposit a 380 nm thick a-Si film on the substrate. In fact, samples were prepared using the sputtering system at the Bell Engineering Centre, University of Arkansas, USA. After deposition, the samples were allowed to cool to room temperature in the vacuum chamber to substantially minimize or prevent film oxidation. A 300 nm thick aluminum film was deposited on top of the a-Si film. In the current study, the Al and a-Si films were arranged in two distinct sequences, as illustrated in Fig. 1, in order to examine the influence of stacking order on the crystallization of the a-Si film. Sample 1 is arranged in the sequence of Al/a-Si/G, with aluminum constituting the uppermost layer. On the other hand, sample 2 is organized as a-Si/Al/G, wherein the aluminum layer is positioned between the amorphous silicon and the glass substrate. Subsequently, the samples were subjected to CW argon-ion (Ar^+) laser, with a wavelength of 514 nm, irradiated from the glass side for sample 1, and from a-Si film side for sample 2, with power densities that extend from 34.4 W/cm^2 to 117.5 W/cm^2. The exposure time of different samples to laser irradiation varied from 10 to 600 seconds. The aluminum film was then etched to allow the examination of the a-Si films by Raman Spectroscopy (Horiba LabRAM HR Raman spectroscope) and SEM (Philips XL30 ESEM) at Arkansas University.

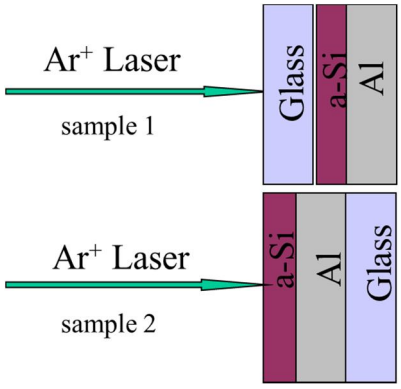

FIG. 1. Diagrams of the configurations used in laser treatment

Results

Raman Spectroscopy Results

Raman spectroscopy is a non-destructive analytical method that provides substantial insights into the structural properties of materials, including crystallinity and defect detection, even in thin film formats. Fig. 2 illustrates the results of irradiated sample 1 subjected to the CW laser with power intensities ranging from 34.4 W/cm² to 117.5 W/cm² for 20 seconds. In the Raman spectrum of single-crystalline or multicrystalline silicon, a peak is present at approximately 520 cm^{-1}. This peak is indicative of the crystal structure of the thin film and corresponds to the first-order optical phonon mode in crystalline silicon. Evidently, the laser intensity influences the peak feature's variation upon a thorough examination of the spectra. At low power levels (34.4–59.8 W/cm²), the Raman spectra show a relatively consistent baseline for the ordinary response of the amorphous thin film. The shape and amplitude of Raman spectra remain somewhat consistent at low powers, specifically within the range of 34.4 to 59.8 W/cm^2. When the laser power is 81.2 or 117.5 W/cm^2, the primary amorphous silicon curve displays distinct peaks with relative heights at a Raman shift of approximately 518 cm^{-1}. This increase is also characterized by a slight peak broadening, which could suggest the occurrence of various structural changes in the thin film, such as the onset of localized heating effects that result in slight changes in the bond length or bond angle of the silicon structure. An alternative explanation is that the increased laser power may have introduced additional thermal tension or strain into the film, potentially resulting in structural variations.

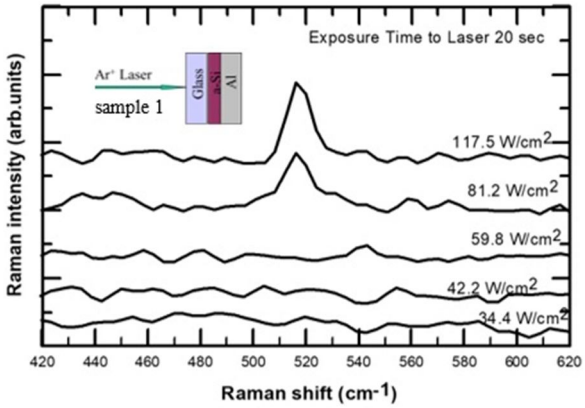

FIG. 2. Raman spectroscopy of silicon thin films exposed to CW laser of variable densities for 20 s.

Figure 3 presents Raman spectroscopy data that provides further understanding of how the silicon thin film acts when the time of exposure to the laser is longer. The spectra shown here were taken at an exposure time of 60 seconds, unlike the earlier 20 seconds, for the same range of laser intensities from 34.4 W/cm^2 to 117.5 W/cm^2. The longer time of exposure better illustrates the changes in structure and properties

that the amorphous silicon thin film undergoes. At lower laser powers (34.4-59.8 W/cm^2), the spectra have a similar baseline to the previous dataset. This consistency at lower intensities indicates that the basic structure of the thin film stays mostly the same, even with longer exposure time in these conditions. With an increase in laser power to 81.2 W/cm^2 and 117.5 W/cm^2, there is a main silicon peak. A stronger response, compared to the 20-second exposure, indicates that longer interaction time results in more noticeable laser effects on the thin film structure.

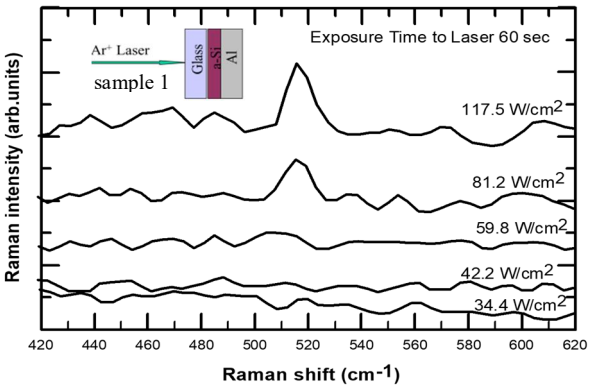

FIG. 3. Raman spectroscopy of silicon thin films exposed to CW laser of variable power densities for 60 s.

The Raman spectroscopy data set in Fig. 4 offers an extensive examination of the behavior exhibited by silicon thin films when subjected to a laser exposure duration of 600 seconds at varying laser intensities. This extended exposure duration uncovers considerable alterations in the structure and properties of the film, thereby providing crucial insights into its long-term stability and reaction to high-intensity laser irradiation. Accordingly, the most striking feature in this data is that which involves the remarkably drastic intensification and broadening of the characteristic silicon peak at around 520 cm^{-1}. Noticeably, this has become pronouncedly strongest at the maximum laser power of 117.5 W/cm^2. This pronounced peak suggests a significant enhancement in Raman scattering efficiency due to possible reasons including more enhanced crystallization and film optical property changes.

In the case of lower laser power levels (34.4 W/cm^2 and 42.2 W/cm^2), no significant change is observed in the Raman spectra. Such an observation points towards any possible threshold effect, beyond which important changes in structure occur. The persistence of key spectral features under these lowered intensities reveals that the amorphous silicon remains largely unchanged.

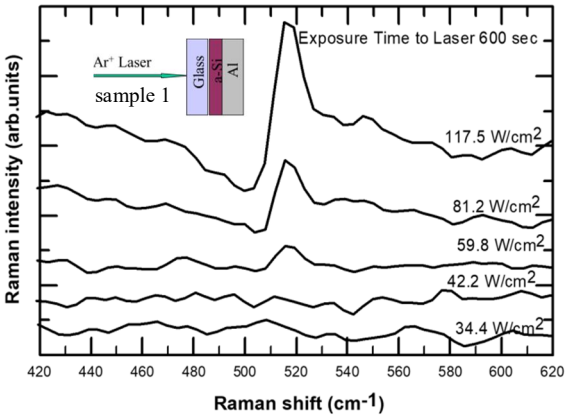

FIG. 4. Raman spectroscopy of silicon thin films after exposure to a CW laser for 600 seconds at different power densities.

Figures 3 and 4 demonstrate that the appearance of a significant Raman peak at around 518 cm^{-1} serves as strong and direct proof of crystallization in the laser-irradiated films. This peak represents the first-order transverse optical (TO) phonon mode of crystalline silicon and is widely acknowledged as a clear indicator of polysilicon production. The extensive Raman band centered at around 480 cm^{-1}, found at reduced laser power densities, is indicative of amorphous silicon. The gradual enhancement and intensification of the 518 cm^{-1} peak with elevated laser power density and extended irradiation duration signify an increased crystalline percentage and enhanced crystalline order.

Remarkably, the spectrum that was measured at 117.5 W/cm^2 had a much higher background intensity across the entire range compared to other lower-power-level spectra. Such a high background could suggest an increased photoluminescence or the onset of thermal radiation, which is evidence of large heating effects in the film at this power level and for this duration of exposure.

Figure 5 shows how crystallization changes with longer exposure times at a constant power density of 117.5 W/cm² in the Raman spectra of laser-treated amorphous silicon thin films. Since it controls the amount of heat dispersion and energy absorption in the material, time plays a crucial role in this process. Shorter exposure durations, like 10 or 20 seconds, allow the laser's energy to start partial crystallization, which

produces smaller crystalline grains embedded in an amorphous matrix. This is demonstrated by the presence of a broad shoulder near 480 cm^{-1}, which is suggestive of residual amorphous silicon, and the broader and less strong peak near 520 cm^{-1}. Larger and more uniform grains grow as the exposure duration increases because of the stored energy that permits more crystallization, as observed at 60 and 600 seconds. As time passes, the 520 cm^{-1} peak becomes sharper and more intense, indicating increased crystallinity and decreased amorphous material. Time drives the slow phase transition at constant power density, providing enough thermal energy to get beyond nucleation barriers and promote grain combination. Long-term exposure guarantees the development of a highly crystalline structure with better uniformity throughout the film surface and fewer grain boundaries. Therefore, time governs the depth and completeness of the crystallization process, whereas power density establishes the intensity of energy given.

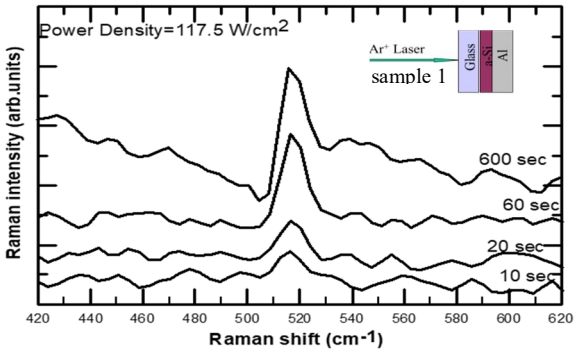

FIG. 5. Raman spectra showing the evolution of crystallinity in laser-treated sample 1 at a constant power density of 117.5 W/cm², with varying exposure time.

SEM Results

Figure 6 presents the SEM image analysis for samples 1 and 2, indicating that the amorphous silicon thin film experienced substantial surface alterations as a result of continuous wave (CW) laser irradiation at 117.5 W/cm² for 10 seconds. Sample 1, consisting of stack Al/a-Si/G, has a distinct nanostructured morphology during SEM inspection. The nanostructures are observed on the surface layer, exhibiting moderate density and somewhat uniform spatial distribution. Nanoscale grain-like textures likely result from the local heating and rapid cooling facilitated by laser-induced modifications. The relatively consistent grain size throughout the field of view indicates either surface diffusion or regulated crystallization. The film's surface has a smooth but grainy texture, characteristic of laser-treated amorphous silicon. The identified structural alterations result from localized melting and re-solidification induced by the dynamic interplay between laser energy and the material layers.

Sample 2, composed of a-Si/Al/G and distinct from sample 1, exhibits a more irregular morphology to laser irradiation, as seen by the denser and more irregularly distributed nanostructures. The reverse arrangement of the layers facilitates direct interaction between aluminum and the laser-induced energy, leading to an increased degree of material mixing. This configuration enhances observable phase transitions by optimizing the rates of thermal conduction and energy absorption. Unlike sample 1, this sample exhibits a broader size distribution and a reduced particle size. The rougher surface of the film indicates a more intense material restructuring during the laser treatment.

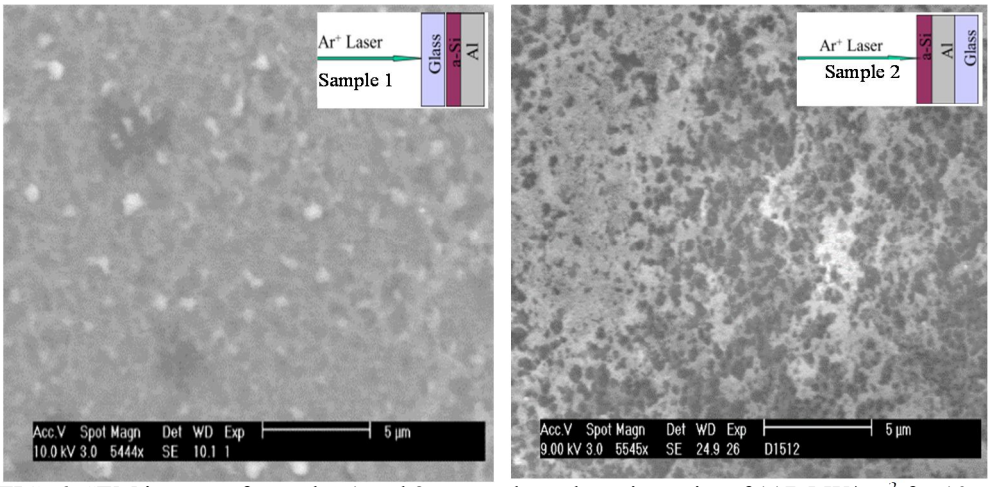

FIG. 6. SEM images of samples 1 and 2 exposed to a laser intensity of 117.5 W/cm^2 for 10 s.

The regularity and density of the nanostructures are the main differences between the two samples. Since the intermediary glass layer modifies energy transfer, sample 1 exhibits a less dense and more organized structure. The configuration of sample 2, on the other hand, results in denser and more irregular grains due to increased energy absorption and more intense material interactions. The spatial arrangement of the layers, which determines the thermal and dynamic reactions during laser exposure, is directly responsible for these variations.

Figure 7 presents the SEM image analysis for both samples, indicating that the amorphous silicon thin film experienced considerable surface alterations as a result of CW laser irradiation at 81.2 W/cm² for 20 seconds. The nanostructural arrangement in sample 1 is consistently dense. Strong interfacial connections and a stable morphology are shown by the tightly bonded structures. The small granular features of the surface coating indicate effective energy absorption during laser irradiation. The relatively tiny grain sizes may enhance the active surface area and augment the optical and electrical properties.

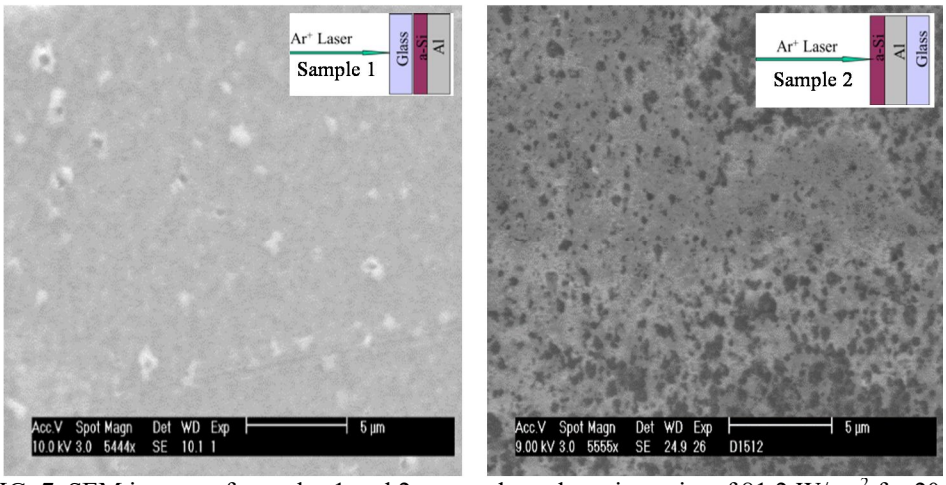

FIG. 7. SEM images of samples 1 and 2 exposed to a laser intensity of 81.2 W/cm^2 for 20 s.

Conversely, sample 2 has a relatively greater nanostructure density due to the inversion of the layer sequence, with glass positioned above. The distribution of nanostructures seems denser, perhaps due to the effect of glass at the upper layer during the laser-induced modification process. This configuration likely alters the thermal dynamics, leading to inhomogeneous structural development and localized hotspots. Compared to sample 1, the grain boundaries are more prominent, suggesting a more heterogeneous surface morphology.

The formation mechanism is governed by laser-induced mechanical and thermal stresses. Structural deformation and thermal dissipation are significantly affected by the layer order. The initial sample is supported by a durable glass substrate, which facilitates the consistent transmission of energy and the organization of its structure. In the second sample, the top glass layer disrupts this homogeneity, resulting in irregular energy propagation and distinct morphological outcomes.

The SEM image analysis in Fig. 8 indicates that the amorphous silicon thin film experienced substantial surface modifications as a result of CW laser irradiation at 59.8 W/cm² for 60 seconds. The nanostructures, surface morphology, and spatial distribution of features of the two samples are evident in the SEM images. These differences can be attributed to their structural composition and exposure to laser irradiation. In sample 1, the surface is relatively smooth and contains small, isolated, and randomly distributed nanostructures. The low density and small particle diameters of these structures indicate that there was only a limited amount of nanostructural formation during laser exposure. The thermal and optical properties of the glass substrate, which absorbs less energy than the a-Si layer, are likely responsible for the minimal rearrangement or melting indicated by the surface morphology. The nanostructures' spatial distribution is irregular, and their dynamic properties indicate a weak interaction between the layers during laser irradiation, resulting in less pronounced structural modifications.

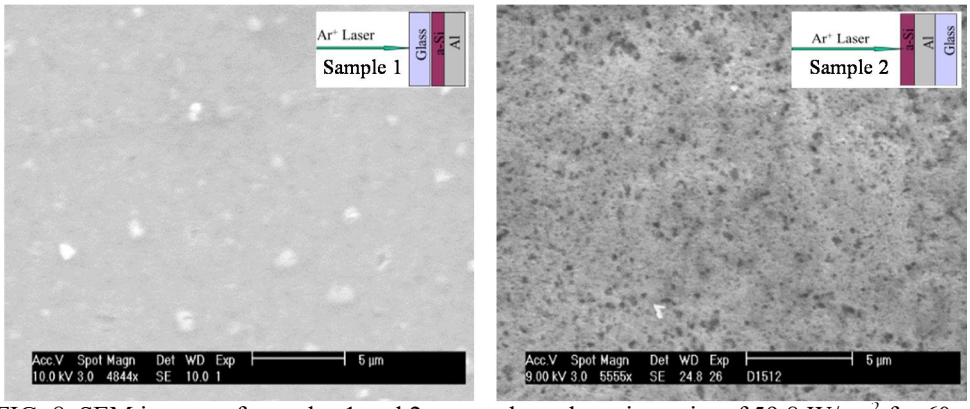

FIG. 8. SEM images of samples 1 and 2 exposed to a laser intensity of 59.8 W/cm^2 for 60 s.

Nevertheless, the surface morphology of sample 2 exhibits a significant difference. The SEM image reveals a more uniformly dispersed substrate with a higher density of nanostructures and a coarser surface. The nanostructures' apparent reduced size and increased number are indicative of the heightened nucleation and growth processes that occur during laser irradiation. The direct exposure of the a-Si layer to the laser energy explains this result, as it facilitates more effective absorption and directed heating. The irregular and densely packed morphology that has been observed may be the result of structural rearrangements and heat transport that are facilitated by the underlying Al layer. The topographical distribution of the nanostructures suggests that the observed features may have been formed by melting and re-solidification processes, which suggests a more dynamic interaction between the layers.

The comparison of the two samples illustrates the critical role of layer configuration in the determination of the surface shape, density of nanostructures, and topographical dispersion. Sample 2 exhibits superior nanostructural characteristics due to its more advantageous energy absorption and heat transfer dynamics. These discoveries underscore the influence of layer organization on the material's response to laser irradiation, which may have implications for applications that require customized nanoscale characteristics.

The SEM images of the two samples are depicted in Fig. 9. The samples were exposed to a CW laser with a power of 59.8 W/cm² for 60 seconds. Due to the distinct layer arrangements and laser irradiation, there are substantial variations in their spatial distribution, surface morphology, and nanoscale properties. The image of sample 1 displays nanostructures that are sparsely disseminated on a comparatively uniform surface. The laser treatment of low power has resulted in minor structural changes, as evidenced by the low density, small size, and isolation of these features. There appears to be little contact between the layers because the nanostructures are randomly dispersed throughout the surface. The smooth appearance indicates that there is insufficient absorption of thermal and optical energy to cause significant melting or rearrangement. This effect could be caused by the layer arrangement or the underlying substrate acting as a thermal insulator, limiting energy transfer and preventing the development of dense nanostructures.

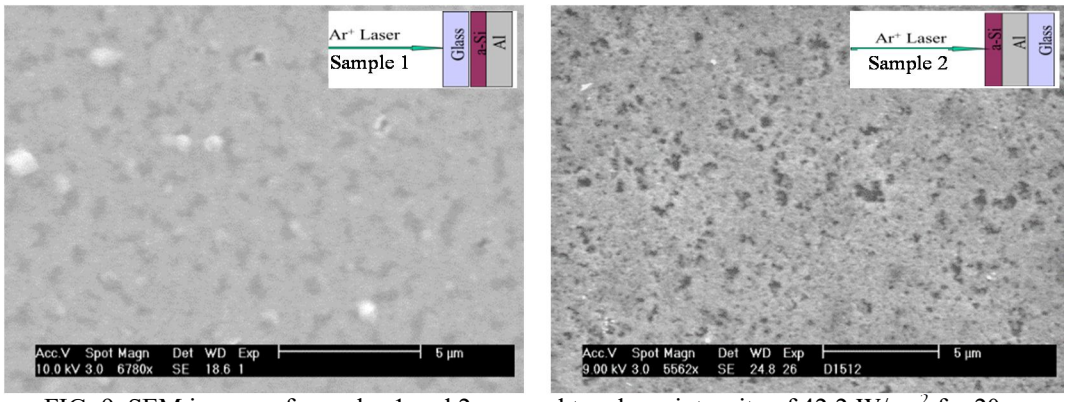

FIG. 9. SEM images of samples 1 and 2 exposed to a laser intensity of 42.2 W/cm^2 for 20 s.

The surface morphology is noticeably rougher and has a higher density of uniformly distributed nanostructures in sample 2. These nanostructures have a higher degree of crystallization and growth processes because they are more numerous but smaller in size. The surface roughness indicates a greater degree of interlayer contact during laser exposure, which likely involves localized melting and resolidification. The shape indicates improved dynamics during the production process, and the spatial distribution of the nanostructures appears more uniform. The structural rearrangement seen in the image may be made possible by layer formation, where the top layer effectively absorbs energy and transfers heat to the underlying layers.

Both samples' layer configurations and their capacity to absorb and transfer energy during laser irradiation have an impact on the mechanism of nanostructure creation. The first sample has sparse and less noticeable nanostructures as a result of the limited absorption and energy transfer. The second sample's consistently dispersed and densely packed nanostructures are made possible by effective heat distribution and absorption. The second sample's reduced grain size suggests that there are more active nucleation sites and quick cooling dynamics, which inhibit excessive grain formation.

Conclusion

This study highlights the role of continuous wave laser irradiation in facilitating the crystallization of amorphous silicon thin films via aluminum-mediated mechanisms. The research establishes that a certain laser power density is required to start crystallization, with further increases in power and duration resulting in increased polycrystalline silicon development. SEM examination indicates substantial microstructural changes, while Raman spectroscopy confirms the gradual enhancement of crystallinity and indicates that longer laser–material interaction times significantly enhance the amorphous-to-polysilicon transformation. This is evidenced by the increased intensity and sharpening of the characteristic 518 cm^{-1} Raman peak, corresponding to a higher crystalline fraction. The configuration of aluminum and silicon layers affects crystallization behavior. These findings give essential direction for enhancing laser-assisted crystallization processes, suggesting potential improvements in semiconductor manufacturing and optoelectronic device applications.

Funding

This research was supported by the Faculty of Scientific Research at Jordan University of Science and Technology (Irbid, Jordan) for research assistance and sample testing under Grant No. 224/2024.

Acknowledgment

The authors would like to express their sincere gratitude to the University of Arkansas for their invaluable support in preparing the films used in this study. Additionally, we gratefully acknowledge the Faculty of Scientific Research at Jordan University of Science and Technology for providing the necessary funding in support of this research.

References

[1] Garcia-Lechuga, M. et al., Laser & Photonics Reviews, 18 (11) (2024) 2301327.

[2] Paduru, S.K. et al., MRS Online Proceedings Library (OPL), 808 (2003) 275.

[3] Ballif, C. et al., Nature Reviews Materials, 7 (2022) 597.

[4] Guo, Z., Liu, Z., and Tang, R., Materials Chemistry Frontiers, 8 (2024) 1703.

[5] Palneedi, H. et al., Advanced Materials, 30 (2018) 1705148.

[6] Aktas, O. and Peacock, A.C., Advanced Photonics Research, 2 (2021) 2000159.

[7] Lim, S.Q. and Williams, J.S., In: Micro (2021), pp.1-22. MDPI.

[8] Lipovka, A. et al., Advanced Optical Materials, 12 (2024) 2303194.

[9] Dutta Majumdar, J. and Manna, I., International Materials Reviews, 56 (2011) 341.

[10] Green, M.A., Semiconductor Science and Technology, 8 (1993) 1.

[11] Jiang, Y. et al., Chemical Society Reviews, 49 (2020) 5885.

[12] Shariah, A., Silicon, 16 (2024) 4461.

[13] Shariah, A. and Bataineh, Mi., Silicon, 15 (2023) 2727.

[14] Hamasha, E. et al., Solar Energy, 127 (2016) 223.

[15] Park, S.J. et al., Thin Solid Films, 511 (2006) 243.